Sign in

AMERICAN METEOROLOGICAL SOCIETY
AMS Journals Online

AMS Home | Journals Home | Journal Archive | Subscribe | For Authors | Help | Advanced Search | Search | Go

Full Text View

Volume 32, Issue 9 (September 2002)

Journal of Physical Oceanography
Article: pp. 2715–2722 | Abstract | PDF (822K)

Long-Term Observations of Tropical Instability Waves

Robert F. Contreras

Department of Atmospheric Sciences, University of Washington, Seattle, Washington

(Manuscript received August 8, 2001, in final form March 18, 2002)

DOI: 10.1175/1520-0485(2002)032<2715:LTOOTI>2.0.CO;2

ABSTRACT

Reynolds sea surface temperature (SST) data showing tropical instability waves (TIWs) in the tropical Pacific are analyzed along with current measurements from the Tropical Atmosphere–Ocean (TAO) buoy array and wind speeds from the *European Remote Sensing Satellite (ERS) -1* and *-2* scatterometers. TIWs are visible as undulations in the SST cold fronts that delineate the northern and southern boundaries of the cold tongue in the equatorial Pacific. The SST pattern results from advection of the SST front by instabilities in the near-surface equatorial currents. Although the waves are seen on both sides of the Pacific cold tongue and north of the equator in the Atlantic, they are most intense, and thereby most observable, in the north equatorial Pacific. The combination of data used in this analysis provides information about these waves, the factors controlling them, and their coupling to the atmosphere on annual and interannual timescales. On annual timescales, the TIWs generally establish a strong signal in July east of about 140°W with a westward phase speed of about 0.5 m s^{-1}. By August, the waves usually occupy the longitudes between 160° and 100°W and continue to propagate west at roughly the same speed. With the onset of the warm season in the equatorial cold tongue (spring), the signal typically weakens and the propagation speeds show large variations. On interannual timescales, activity is strongest during the cold phase of the ENSO cycle (La Niña) when the cold tongue is most pronounced; the waves are weak or nonexistent during the warm phase of ENSO (El Niño) when the SST front is weak. The TIW signature in SST is noticeable throughout all seasons of the year provided that the gradient in SST at 140°W is greater than about 0.25°C (100 km) $^{-1}$. In addition, analysis of the currents underlines the importance of the background currents to the zonal propagation speeds.

Options:
- Create Reference
- Email this Article
- Add to MyArchive
- Search AMS Glossary

Search CrossRef for:
- Articles Citing This Article

Search Google Scholar for:
- Robert F. Contreras

1. Introduction

In the Pacific, intense tropical instability waves (TIWs) occur along the sea surface temperature (SST) front that marks the northern boundary of the equatorial cold tongue. TIWs are visible as cusplike perturbations in this SST front. Weaker TIWs have been noted on the southern edge of the Pacific cold tongue and also at 1°N in the Atlantic (Chelton et al. 2000). In the northern Pacific, they were first noted in infrared images of the sea surface in 1975 by Legeckis (1977), and their westward phase speed was estimated to be about 0.5 m s^{-1}. Figure 1 shows the mean SST in the equatorial Pacific for the week of 11 October 1998. Evident in the figure are the SST cold tongue, the SST cold front, and undulations in the front that are the TIWs. The cold tongue is typically centered at about 1°S, with the SST front centered at about 2°N (Wallace et al. 1989). This front also marks a region of intense shear in the surface and near-surface currents; the eastward North Equatorial Countercurrent meets the westward South Equatorial Current (SEC) at about 4°N (Gill 1982). Just south, within 1° north or south of the equator, the SEC overlies the Equatorial Undercurrent (EUC). In Qiao and Weisberg (1998), the authors discuss modeling studies that have implicated both the shear and SST gradients in the existence of TIWs, but they conclude that, just north of the equator, the waves arise from and are maintained by barotropic instability associated with cyclonic shear within the SEC and EUC.

The spatial perturbations in SST associated with these waves couple the atmospheric boundary layer (ABL) to oceanic TIWs. This was first noted in Hayes et al. (1989) when the authors did temporal correlations of differences in surface winds (2°N–equator and equator–2°S) and SST from an array of moored sensors. They observed significant correlations in the wind speed associated with TIWs, with wind speed perturbations as large as 1–2 m s^{-1}. The authors postulated that the coupling of the ABL to the TIWs could be accomplished by hydrostatic sea level pressure perturbations, changes in the ABL stratification, or a combination of the two. As a result of the phase relationship they observed between SST and near surface wind velocity perturbations, the authors concluded that the coupling was dominated by the changes in stratification. As the air travels in a southeasterly direction over the equatorial cold tongue, it travels from colder upwelled water to warmer water. Over the colder water, the ABL is stably stratified and the vertical flux of horizontal momentum is inhibited. The near-surface winds increase as the stratification becomes more unstable over warmer water and more horizontal momentum is mixed down. Using an atmospheric general circulation model and imposing an SST field similar to that associated with TIWs, Xie et al. (1998) reproduced atmospheric wind anomalies consistent with those observed by the *European Remote Sensing Satellite (ERS)-1* scatterometer. In doing so, the authors further supported the role of stratification in coupling the atmosphere to the ocean as hypothesized by Hayes et al. (1989). As described in Wentz et al. (2000), the Tropical Rainfall Measuring Mission (TRMM) Microwave Imager (TMI) has provided SST measurements at sufficient resolution to enable a concise description of TIWs in all but raining weather conditions. Used in conjunction with the surface winds measured by the Seawinds scatterometer on the Quick Scatterometer (QuikSCAT) Satellite, the TMI SST measurements have allowed Liu et al. (2000), Chelton et al. (2001), and Hashizume et al. (2001) to describe these waves further and to investigate their air–sea coupling mechanism, which has significant implications for air–sea interactions. Because the scatterometer infers winds from the roughness of the ocean surface, and the roughness is dictated by the difference between the wind and the surface current, scatterometer winds have the surface currents implicit in them (Kelly et al. 2001). Given this fact and the fact that the currents associated with TIWs are so large (Halpern et al. 1988), it is likely that the TIW signature in the scatterometer wind field is a combination of the surface currents and near-surface winds. In fact, Polito et al. (2001) found that the surface currents make up a significant portion of the QuikSCAT wind anomalies associated with TIWs. This situation probably has added to the uncertainty in the phase relationships noted by Liu et al. (2000) and Hashizume et al. (2001) and has been suggested in Chelton et al. (2001) as the reason for differences in their coupling terms. Regardless of this distortion, the signature seen in the ERS scatterometers is clear and can be used to verify the existence and phase speed of the oceanic TIWs seen in the SST.

The purpose of this note is to establish a comprehensive picture of TIWs by using various data sources from 1992 to 2000. Here, perturbations in the SST will be used to identify the TIWs because they provide a long record and play a significant role in the atmosphere–ocean coupling. It should be kept in mind that the SST signature of these waves can possibly persist after the velocity perturbations have subsided. That is, once the SST front has been advected north or south, the corresponding SST perturbations will remain until they are further advected around, dissipated by turbulence, or dissipated by the differential radiative heating associated with low-cloud formation over the warm SST anomalies (Deser et al. 1993). The data used in this study are the Reynolds SST, *ERS-1* and *-2* scatterometer measurements, and currents from the Tropical Atmosphere Ocean (TAO) buoys. The datasets will be discussed in section 2. Then, the annual and interannual behavior of TIWs will be presented, with the role of ENSO being emphasized, in section 3. In section 4, the relationship between the onset of the waves, their zonal propagation, and the background SST gradient and current will be presented. In section 5, the behavior of TIWs will be summarized and the role of the background fields will be discussed.

2. Data

The SST data used here are referred to as Reynolds SST data after the optimum interpolation method (Reynolds and Smith 1994) used to create 1° × 1° gridded weekly means. The Reynolds SST data were provided by the National Oceanic and Atmospheric Administration (NOAA)–Cooperative Institute for Research in Environmental Sciences Climate Diagnostics Center in Boulder, Colorado, from their Internet site (http://www.cdc.noaa.gov/). Even though the Reynolds SST data do

not show the sharp features in SST associated with TIWs noted in Chelton et al. (2000), they do show the waves, and the long record of this dataset makes it ideal for studying TIWs on interannual timescales. In the following analysis, time–longitude plots (or Hovmöller diagrams) of the SST at 2.5°N between 160.5°E and 80.5°W are used to show TIWs. The horizontal line in Fig. 1 at 2.5°N indicates the domain of the time–longitude plots. The data at 2.5°N are shown, as opposed to those at 0° (at which latitude the buoy measuring currents is located), because the wave signal was strongest at this latitude and there were no appreciable differences in the phase speeds between the two latitudes. A comparison of phase speed estimates is shown in Fig. 2. SST data and constant phase estimates are shown at 2.5°N (Fig. 2a) and at the equator (Fig. 2b). The phase speeds calculated from these constant phase estimates are shown in Fig. 2c, and, as we can see, the differences at the two latitudes are small. In addition to the time–longitude plots, the differences in SST at 140° W between 4.5° N and 0.5° N were used to investigate the relationship between SST gradient and the existence of the waves. The SST values at both latitudes were 12° longitudinal means centered at 140°W; 12° is roughly the wavelength of TIWs.

The *ERS-1* and *-2* scatterometers give wind vector measurements with 50-km resolution, and they cover 40% of the global ocean daily. Although the sparsity of these data introduces sampling errors when considering waves with periods as short as 20 days (Halpern et al. 1988), the waves are often visible, with clearly discernible phase speeds. As mentioned earlier, Xie et al. (1998) found agreement between these data and GCM-simulated wind perturbations in their study of TIWs. The data used here were provided by the French Institute for the Research and Exploitation of the Sea (IFREMER) from their Internet site (http://www.ifremer.fr/). The data have been interpolated in space and time to provide 1° × 1° weekly gridded means using a minimum variance method similar to the Kriging technique. In the tropical Pacific, the annual cycle is the greatest source of variance in the surface winds, often obscuring the signal of TIWs. Therefore, sine and cosine functions with periods of 12, 6, and 4 months were fit to the data in a least squares sense and removed.

To compare the phase speed of the waves with the underlying surface current, SST and scatterometer data showing the waves were used in conjunction with moored current measurements. The current data were provided by the TAO project at NOAA/Pacific Marine Environmental Laboratory. Fixed current-meter and upward-looking ADCP measurements were used from the buoy at 0°N, 140°W. The time period analyzed here was January of 1992–July of 2000. During this period, the best current measurements, those that were the most continuous and the closest to the surface, were the fixed current meter measurements at 10-m depth and the ADCP measurements at 25- and 30-m depth. When possible, the currents at 10-m depth will be displayed along with the mean of those at 25 and 30 m.

To establish mean (or background) conditions, both the SST gradient and the currents have been low-pass filtered with a cutoff period of 20 weeks. Such a long period was chosen because the TIWs often displayed considerable slowing in their propagation and it was desirable not to include these lower-frequency TIW perturbations in the background quantities.

3. Climatological description

TIWs are visible as undulations in the SST front. Therefore, their activity is tied to the annual and interannual cycle of the cold tongue. Because the state of the cold tongue is dominated by the El Niño–Southern Oscillation, a dependence of TIW activity on ENSO is expected. When ENSO is in its warm phase, El Niño, the easterly/southeasterly trade winds weaken and equatorial upwelling is decreased. As a result, the strength of the SST front is diminished. During the opposite phase, La Niña, the conditions reverse, and the SST front is strengthened. Anomalies in the SST are often used as a measure (or index) of the phase of ENSO. Figure 3 is a time series of the weekly mean SST anomalies within the area 5°N–5°S and 150°–90°W and is one such index.

Figures 4, 5, and 6 are series of time–longitude (Hovmöller diagrams) and time series plots organized according to the phase of ENSO. Figure 4 corresponds to a period when ENSO was in neither an extreme warm phase nor an extreme cold phase, neither El Niño nor La Niña. Figure 5 corresponds to an El Niño period, Fig. 6 to a La Niña period. The purpose of these figures is to show the TIWs, the atmospheric response to them, and the conditions that control their behavior for the different phases of ENSO. In each series of figures, those labeled “a” are the Reynolds SST; TIWs are readily visible in this field. To show the atmospheric coupling to the SST, scatterometer wind speeds are shown in “b.” And to investigate the influence of the background fields on TIWs, SST gradients are shown in “c” and currents are shown in “d.”

Except for the El Niño year, 1997, Figs. 4a, 5a, and 6a show that the waves generally establish a strong signal in July east of about 140°W that propagates west at about 0.5 m s^{-1}. By August, the waves usually occupy the longitudes between 160° and 100°W and continue to propagate west at roughly the same speed. During these times, the waves are also visible in the scatterometer winds. The warm season in the equatorial cold tongue follows this period of strong wave activity, and the waves often slow and weaken in intensity. At times TIWs vanish altogether; examples are in April of 1992 and April of 2000.

Except for the first few months during which time there was a weak El Niño, the data shown in Figs. 4a, 4b, 4c, and 4d correspond to periods when ENSO was in neither an extreme warm phase nor an extreme cold phase and are indicative

of a “typical” period. Throughout this period, the TIWs were clearly visible in the SST data (Fig. 4a), with their intensity being seasonally modulated; the waves were most intense during the cold season in the equatorial cold tongue and were weak or nonexistent during the warm season. Of interest, the SST signature of the waves often continued from one season to the next. Wave activity starting in 1993 lasted throughout the rest of the period shown in the figure, weakening during the 1994 and 1995 warm seasons but not disappearing. During these periods of weakening, considerable variations in the westward propagation speed are also apparent.

As mentioned above, the SST field shown in Fig. 4a began during El Niño conditions, at which time no TIWs were visible. With the onset of the following El Niño in 1997 shown in Fig. 5a, the SST cold tongue virtually disappeared and the TIW activity ceased. Strong El Niño conditions eliminate the cold front and weaken the EUC (Firing et al. 1983). Therefore, El Niño conditions remove the medium upon which TIWs are visible and decrease the source of energy for the instabilities.

Following the El Niño in 1997, conditions reversed and La Niña conditions lasted for roughly two years. The SST field for the La Niña years (Fig. 6a) shows intense TIW activity that continued from the 1998/99 wave season through the 1999/2000 wave season. The enhanced cold front associated with La Niña conditions makes the undulations in it, the TIWs, more noticeable. In addition, increased shear likely exists in the currents, providing a greater source of energy for the growing instabilities.

4. Onset and westward propagation

The 9-yr record of the data used here enables us to develop a comprehensive picture of TIWs. Analysis of the waves visible in SST data, along with the gradient in SST and the near-surface currents at 140°W, sheds light upon the factors controlling both their onset and zonal propagation.

a. Onset

It has been accepted that, near the equator, TIWs primarily result from barotropic instability, receiving their energy from shear and not from SST gradients. Nevertheless, the gradient in SST across the cold front is extremely useful in analyzing the waves for a few reasons. First, SST measurements are relatively easy to make, providing us with an extensive dataset in both time and longitude. Second, TIWs are undulations in the SST front, and, as a result, their signature is very noticeable in the field. Last, because both current shear and upwelling near the equator are driven by wind-created surface stress, the SST front resulting from the upwelling can be used as an index of the shear. Comparing the time–longitude SST (Figs. 4a, 5a, and 6a) with the gradient of SST at 140°W (Figs. 4c, 5c, and 6c) illuminates the relationship between TIWs and the SST gradient. TIWs were visible in the SST data for all times that corresponded to meridional gradients greater than about 0.25°C (100 km)$^{-1}$.

b. Westward propagation

Quite clear in the figures of Reynolds SST (Figs. 4a, 5a, and 6a) were TIWs that showed significant deviations from the ~0.5 m s^{-1} first noted by Legeckis (1977). Shown in these figures of SST are estimates of constant phase lines from which propagation speeds shown in Figs. 4d, 5d, and 6d were deduced. Figure 7 is a histogram of estimates of the phase speed of the waves. Deviations often occurred during the equatorial warm season. In the literature, variations in the zonal propagation speed have often been noted. In one example, Chelton et al. (2001) noted deviations in time and in different geographic locations. The SST data shown in Fig. 6a overlap those analyzed in Chelton et al. (2000, 2001). The signal of TIWs is clearly visible. The propagation of TIWs at 140°W in November of 1998 was about 0.5 m s^{-1}, which is in agreement with Chelton et al. (2000). The waves propagated at this speed until February. At that time, the phase speed decreased and reached a minimum of about 0 m s^{-1} in about April of 1999. Coincident with the slowing of the TIWs in February was an enhanced zonal current. As shown in Fig. 6d, the current at 25–30-m depth began to increase in February and reached a maximum of about 1 m s^{-1} in May. At this time, the 10-m currents became large and eastward until the current meter stopped functioning. It was unfortunate that the current meter at 10-m depth stopped functioning prior to the changes in the currents and TIW propagation that occurred in about May of 1999, because these currents were so large and the waves were so apparent. The addition of the 10-m current measurements would have given an idea of the shear with height that is often found in the near-surface equatorial currents and therefore would have given a better idea of the current structure affecting the TIWs. Regardless, the simultaneous occurrence of the changes in the propagation speed of the TIWs and the zonal current suggests that the background current is affecting the westward propagation of these waves.

The currents at 10-, 25-, and 30-m depth were measured at other times of notable TIW slowing. For example, the waves shown in Fig. 4a, exhibit a substantial change in their propagation from April of 1994 to July of 1994 and from April of 1995 to July of 1995. The mean current at 25- and 30-m depth showed a corresponding change, becoming increasingly eastward. Similar changes were also seen in the 10-m measurements. The combination of these current data shows a

westward shear with height in the near-surface currents that suggests a westward surface current greater than that at 10 m. The facts that the near-surface currents and phase speed estimates are comparable and that there are simultaneous fluctuations in both suggest that the SEC is a key element in the observed propagation speeds of TIWs.

5. Summary and discussion

TIWs are typically most intense between 160° and 100°W, from July through the end of the year, and they tend to propagate westward at about 0.5 m s^{-1}. On interannual timescales, the waves vary in concert with the phase of ENSO. Activity is strongest during the cold phase (La Niña) when the cold tongue is most pronounced, and the waves are weak or nonexistent during the warm phase (El Niño) when the SST front is weak. Coincident with the strong signature of these waves in the SST is the signature in the scatterometer winds, which is probably a combination of the stratification-induced coupling noted by Hayes et al. (1989) and modified surface stress resulting from the surface currents, as discussed in Polito et al. (2001).

TIWs have been previously noted to have a well-defined season: starting about May with the enhanced cold tongue and terminating at about the end of the year. The length of the records used here has allowed us to observe the TIW SST signature persisting from one wave season to the next. TIWs were clearly visible whenever the background SST gradient at 140°W was greater than 0.25°C $(100\ km)^{-1}$. April of 1999 is an example of a period during which the waves weakened but did not vanish. Coincident with this weakening, the zonal propagation of the waves decreased to roughly 0 m s^{-1}. Analysis of the TIW propagation speeds and the background currents at 10, 25, and 30 m suggests that the zonal propagation of the TIWs is intimately linked to the background current. It is important to reiterate here that the SST signature of the waves may behave differently than the velocity perturbations, persisting after the velocity perturbations have died off. As a result, the TIW signature may simply be the remnant of previous instability waves and may not be associated with zonal or meridional velocity perturbations. If this is the case and the SST signature is simply persisting after the dynamical signature has terminated, it is expected that the propagation speeds observed at 2.5°N during these times are the result of advection by the background current.

Possible explanations as to why the continuation of the waves from season to season and the large fluctuations in their propagation speeds have not previously been noted include the following: these phenomena are exclusive to the SST anomalies and are not present in the velocity perturbations, which have been the focus of many studies; the periods of observation have been short, and these phenomena simply have not been seen; and the waves have been filtered out of the data during periods of their reduced phase speeds. Because variations in SST and wind speed in the tropical Pacific are dominated by the annual and interannual cycles, it has been desirable to filter out these low-frequency variations when looking for TIWs. However, high-pass filtering these time series with a cutoff period of less than 3 or 4 months removes the TIW signal during times of slow propagation.

As mentioned earlier, the growing periods of observation by satellite instruments such as the QuikSCAT scatterometer and the TRMM TMI will enable us to characterize the behavior of TIWs and to develop a precise understanding of the role of TIWs in the ocean–atmosphere system. In addition, combining these data with long-term current measurements will illuminate the equatorial dynamics that underly TIWs.

Acknowledgments

The author is extremely grateful to John M. Wallace and William J. Plant for their encouragement and guidance. This work was supported in part by ONR AASERT Grant N00014-97-1-0708.

REFERENCES

Chelton D. B., F. J. Wentz, C. L. Gentemann, R. A. de Szoeke, and M. G. Schlax, 2000: Satellite microwave SST observations of transequatorial tropical instability waves. *Geophys. Res. Lett.*, **27**, 1239–1242. Find this article online

Chelton D. B., Coauthors, 2001: Observations of coupling between surface wind stress and sea surface temperature in the eastern tropical Pacific. *J. Climate*, **14**, 1479–1498. Find this article online

Deser C., J. J. Bates, and S. Wahl, 1993: The influence of sea surface temperature gradients on stratiform cloudiness along the equatorial front in the Pacific Ocean. *J. Climate*, **6**, 1172–1180. Find this article online

Firing E., R. Lukas, J. Sadler, and K. Wyrtki, 1983: Equatorial undercurrent disappears during 1982–1983 El Niño. *Science*, **222**, 1121–1123. Find this article online

Gill A. E., 1982: *Atmosphere–Ocean Dynamics*. Academic Press, 482–483.

Halpern D., R. A. Knox, and D. S. Luther, 1988: Observations of 20-day period meridional current oscillations in the upper ocean along the Pacific equator. *J. Phys. Oceanogr.*, **18**, 1514–1534. Find this article online

Hashizume H., S.-P. Xie, W. T. Liu, and K. Takeuchi, 2001: Local and remote atmospheric response to tropical instability waves: A global view from space. *J. Geophys. Res.*, **106**, 10173–10185. Find this article online

Hayes S. P., M. J. McPhaden, and J. M. Wallace, 1989: The influence of sea-surface temperature on surface wind in the eastern equatorial Pacific: Weekly to monthly variability. *J. Climate*, **2**, 1500–1506. Find this article online

Kelly K. A., S. Dickinson, M. J. McPhaden, and G. C. Johnson, 2001: Ocean currents evident in satellite wind data. *Geophys. Res. Lett.*, **28**, 2469–2472. Find this article online

Legeckis R., 1977: Long waves in the eastern equatorial Pacific Ocean: A view from a geostationary satellite. *Science*, **197**, 1179–1181. Find this article online

Liu W. T., X. Xie, P. S. Polito, S.-P. Xie, and H. Hashizume, 2000: Atmospheric manifestation of tropical instability wave observed by QuikSCAT and Tropical Rain Measuring Mission. *Geophys. Res. Lett.*, **27**, 2545–2548. Find this article online

Polito P. S., J. P. Ryan, W. T. Liu, and F. P. Chavez, 2001: Oceanic and atmospheric anomalies of tropical instability waves. *Geophys. Res. Lett.*, **28**, 2233–2236. Find this article online

Qiao L., and R. H. Weisberg, 1998: Tropical instability wave energetics: Observations from the Tropical Instability Wave Experiment. *J. Phys. Oceanogr.*, **28**, 345–360. Find this article online

Reynolds R. W., and T. M. Smith, 1994: Improved global sea surface temperature analysis using optimum interpolation. *J. Climate*, **7**, 929–948. Find this article online

Wallace J. M., T. P. Mitchell, and C. Deser, 1989: The influence of sea-surface temperature on surface wind in the eastern equatorial Pacific: Seasonal and interannual variability. *J. Climate*, **2**, 1492–1499. Find this article online

Wentz F. J., C. Gentemann, D. Smith, and D. Chelton, 2000: Satellite measurements of sea surface temperature through clouds. *Science*, **288**, 847–850. Find this article online

Xie S.-P., M. Ishiwatari, H. Hashizume, and K. Takeuchi, 1998: Coupled ocean–atmosphere waves on the equatorial front. *Geophys. Res. Lett.*, **25**, 3863–3866. Find this article online

Figures

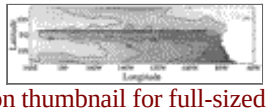

Click on thumbnail for full-sized image.

FIG. 1. Weekly mean SST in the tropical eastern Pacific for the week of 11 Oct 1998. The SST contours are 22°, 24°, 26°, and 28° C. The horizontal line at 2.5°N marks the position of the time–longitude plots (see Figs. 4a,b; 5a,b; and 6a,b)

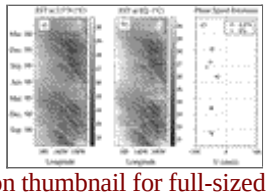

Click on thumbnail for full-sized image.

FIG. 2. Reynolds SST at (a) 2.5° N and (b) the equator. Also plotted are estimates of constant phase lines. (c) Phase speeds determined from constant phase estimates of (a) and (b)

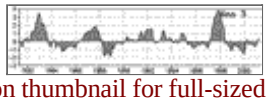

Click on thumbnail for full-sized image.

FIG. 3. Time series of SST anomalies within the Niño-3 area: 5°N–5°S, 150°–90°W. On the ordinate the anomaly in SST is shown in degrees Celsius

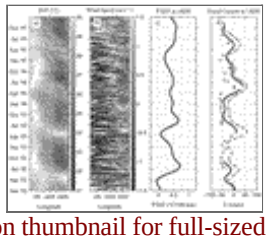

Click on thumbnail for full-sized image.

FIG. 4. (a) Reynolds SST from 1 Jan 1992 through 31 Dec 1995, when ENSO was not in an extreme phase. The range of SST is 21°–30°C (white). Also plotted are estimates of phase lines. (b) Wind speed anomalies from the *ERS-1* scatterometer ranging from −2.5 to 2.5 m s^{-1}. (c) The gradient in background SST between 4.5°N and 0.5°N at 140°W. The means of SST span 12° of longitude and are centered at 140°W. (d) Zonal current at 140°W and estimates of TIW phase speed: mean of 25- and 30-m-depth ADCP measurements (dashed), 10-m current meter measurements (solid), and phase speed estimates (+)

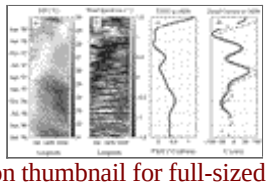

Click on thumbnail for full-sized image.

FIG. 5. Same as Fig. 4 but from 1 Jan 1996 through 30 Jun 1998, an El Niño period

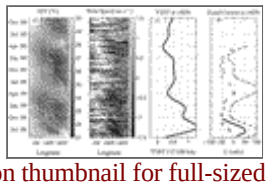

Click on thumbnail for full-sized image.

FIG. 6. Same as Fig. 4 but from 1 Jul 1998 through 31 Dec 2000, a La Niña period

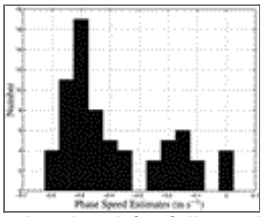

Click on thumbnail for full-sized image.

FIG. 7. Histogram of phase speed estimates from Figs. 4a, 5a, and 6a. Eastward phase speeds are positive, and westward phase speeds are negative

Corresponding author address: Robert F. Contreras, Dept. of Atmospheric Sciences, 408 Atmospheric Sciences–Geophysics Bldg., University of Washington, Box 351640, Seattle, WA 98195-1640. E-mail: robb@apl.washington.edu

top

© 2008 American Meteorological Society Privacy Policy and Disclaimer
Headquarters: 45 Beacon Street Boston, MA 02108-3693
DC Office: 1120 G Street, NW, Suite 800 Washington DC, 20005-3826
amsinfo@ametsoc.org Phone: 617-227-2425 Fax: 617-742-8718
Allen Press, Inc. assists in the online publication of *AMS* journals.